A Skull Stripping Method Using Deformable Surface and Tissue Classification

Xiaodong Tao and Ming-Ching Chang

GE Global Research Center, One Research Circle, Niskayuna, NY 12309
{taox, changm} @ge.com

ABSTRACT

Many neuroimaging applications require an initial step of skull stripping to extract the cerebrum, cerebellum, and brain stem. We approach this problem by combining deformable surface models and a fuzzy tissue classification technique. Our assumption is that contrast exists between brain tissue (gray matter and white matter) and cerebrospinal fluid, which separates the brain from the extra-cranial tissue. We first analyze the intensity of the entire image to find an approximate centroid of the brain and initialize an ellipsoidal surface around it. We then perform a fuzzy tissue classification with bias field correction within the surface. Tissue classification and bias field are extrapolated to the entire image. The surface iteratively deforms under a force field computed from the tissue classification and the surface smoothness. Because of the bias field correction and tissue classification, the proposed algorithm depends less on particular imaging contrast and is robust to inhomogeneous intensity often observed in magnetic resonance images. We tested the algorithm on all T1 weighted images in the OASIS database, which includes skull stripping results using Brain Extraction Tool; the Dice scores have an average of 0.948 with a standard deviation of 0.017, indicating a high degree of agreement. The algorithm takes on average 2 minutes to run on a typical PC and produces a brain mask and membership functions for gray matter, white matter, and cerebrospinal fluid. We also tested the algorithm on T2 images to demonstrate its generality, where the same algorithm without parameter adjustment gives satisfactory results.

Keywords: Magnetic Resonance Imaging, Deformable Surface Model, Tissue Classification, Skull Stripping

1. INTRODUCTION AND BACKGROUND

Extraction of brain tissue from magnetic resonance (MR) images, commonly known as skull stripping, is an important first step of many neuroimaging applications, including cortical surface reconstruction.[1] The goal of skull stripping is to segment the image space into brain tissue and extracranial tissue. The problem of skull stripping is difficult due to the different contrasts of the MR images, the inhomogeneous intensity introduced by the non-uniformity of the B_0 magnetic field, the complex geometry of the brain, and the connections between brain and surrounding non-brain tissue. Different neuro imaging applications have different requirements in the performance of the skull stripping process. For example, morphological analysis of cortex[2,3] requires relatively more accurate skull stripping that has clean separation of brain from not only the skull, but also the dura matter and the vescular structures. Applications targeted at brain visualization[4] and white matter analysis[5,6] typically have more relaxed accuracy requirement.

There have been some algorithms reported in literature. Fennema-Notestine *et al*[7] performed quantitative comparison of four automated algorithms, summarized the advantages and disadvantages of each algorithm, and suggested to form a meta algorithm for skull stripping. The skull stripping algorithms in the literature can roughly be classified as:

(i) Deformable surface based algorithms,[8] where surface models evolve under the influence of the image intensity and surface tension, which maintains the topology and smoothness of the surface. In this catagory, the image force that defines the deformation of the surface is typically derived from the image intensity. In the case of magnetic resonance imaging, different contrasts are used in different imaging protocols. Therefore the external force term depends on the MR contrast mechanism. Also, MR images usually exhibit smoothly varying inhomogeneity, which modulates image contrast at different part of the image and makes it difficult to define a uniform image force that works for the entire image.

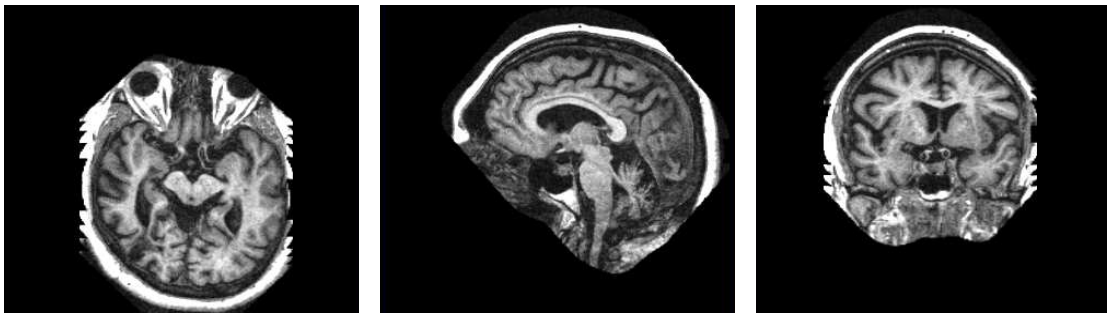

Figure 1. Three orthogonal views of an example dataset from OASIS database.

(ii) Morphological operation based algorithms,[9,10] where morphological dilation and erosion are repeated until brain is isolated from the extracranial tissue based on certain criteria. Because of the complex connectivity of the brain tissue and non-brain tissue and the aforementioned inhomogeneity, human intervention is often required at the end of the process to correct for the automated results.

(iii) Deformable template based algorithms,[11] where a template MR image with ground truth segmentation is registered to the image being segmented and the ground truth segmentation of the template is transferred to the image space. The accuracy of this approach is dependent on the accuracy of the registration process, which is a common issue with segmentation using registration. In this catagory, multiple templates may be used, where skull stripping results from all the template registrations are combined by a voting scheme.

(iv) Hybrid algorithms combining more than one of the above techniques.[12,13] For example, in,[13] an atlas with a ground truth segmentation is first registered to the subject image to create an initial brain mask. Then a series of morphological operation and voxel-wise analysis steps is applied to remove non-brain voxels from this mask, and add brain voxels back.

Our algorithm is a deformable surface based algorithm. It uses tissue classification and bias field estimation to compute external force for surface deformation and relies on internal force derived from local surface patch to maintain the topology and smoothness of the surface.

2. METHODS

In this section, we describe the details of our algorithm, which include an initialization step, a iterative tissue classification and inhomogeneity correction step, and a surface deformation step.

2.1 Pre-processing

Before applying the skull stripping algorithm, we first transform the brain volume into axial orientation and identify the axial slices that include the entire brain. We first compute the maximal intensity of each axial slice to find the top of the head and then extract only slices within a distance from the top slice. Empirically, we set this distance to 160 mm. This step, although not critical, exclude most of the jaw and neck from our process and gives a better initialization in the next step. Figure 1 shows three orthogonal views of an example dataset from OASIS database.

2.2 Histogram Based Initialization

In the initialization step, we define an ellipsoid that include only the brain tissue. A histogram is computed to determine the initial threshold to separate the brain from background. Every voxel with an intensity above this threshold is considered as the foreground and is contributing to the initial computation of the brain centroid, which provides an approximation of the brain location. The initial ellipsoidal surface is represented explicitly as a triangular mesh centered at the initial centroid. The dimensions of this ellipsoidal surface depend on the head size estimated from the thresholded image. As the surface evolves, the geometry of this initial surface has little effect on the final segmentation result, as long as the initial surface lie inside the brain tissue. Figure 2 shows a typical initialization.

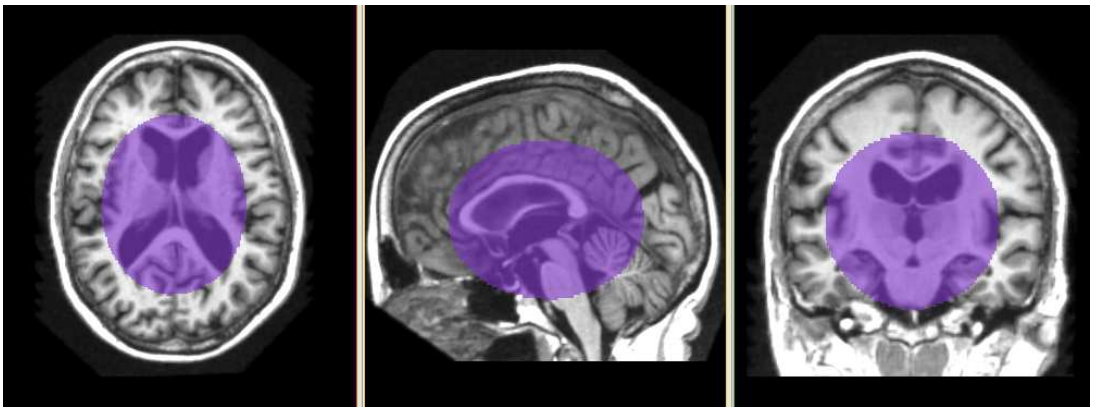

Figure 2. Histogram based initialization. Region inside the ellipsoid is used for estimation of mean intensity of each tissue class and a smooth inhomogeneity field.

2.3 Tissue Classification and Inhomogeneity Correction

The above ellipsoidal surface also serves as a mask within which a tissue classification algorithm is applied. The tissue classification uses a fuzzy clustering algorithm with a parametric bias field model.[14] It assigns membership values of gray matter (GM), white matter (WM), and cerebrospinal fluid (CSF) and estimates a smooth multiplicative bias field at each voxel inside the mask.

Our approach follows the Adaptive Fuzzy C-Mean (AFCM) paradigm[15] with a different solution in correcting the inhomogeneous gain field using parametric *regression fitting*. We assume the true underlying image without inhomogeneities to be the product of a *smooth* gain field (or bias field) g with the observed image. We estimate g together with tissue labelling in an integrated process, which iterates on two main steps — a fuzzy clustering step for tissue labelling and a gain field estimating step for intensity correction. The iteration stops when both the gain field estimation and the tissue labelling converge. The major difference in our approach to[15] is on how the gain field is estimated. Our novelty is to use a simple regression method to correct a smooth bias field via parametric fitting. Our fuzzy clustering step mimics the original Fuzzy C-Mean (FCM) algorithm,[16] which in particular can be applied in any region of interest. We use a set of membership functions $\{u_k\}$ to characterize the likelihood of which each voxel belongs to a certain tissue class, where u_k takes values between 0 and 1. If the intensity of a voxel is close to the prototypical centroid v_k of a class, its membership value is high (close to 1), indicating this voxel should belong to this class. The summation of all classes of $\{u_k\}$ in each voxel is always 1.

The result of tissue classification and bias field estimation is then extrapolated into the entire image including extracranial tissue. Because the inhomogeneity field is estimated as a parametric surface using regression. The extrapolation of inhomogeneity field and tissue classification is straightforward. First the smooth parametric inhomogeneity field is removed from the image. Then the inhomogeneity corrected centroids for tissue classes are applied to the entire image.

The benefits of using the tissue classification step are: *(i)* by applying bias field correction, we eliminate the location dependent variation in the image intensity, and make the computation of the forces for deformation more accurate and robust; *(ii)* by working with tissue membership functions, rather than image intensity, we make the algorithm independent of different contrasts produced by different MR image protocols. Note that neuro images with all contrasts do not warrant separation between gray matter and white matter. As long as our assumption holds that contrast exists between brain tissue (union of GM and WM) and CSF, the skull stripping algorithm will be able to find the interface that includes only the brain tissue.

2.4 Surface Deformation

The next step in our skull stripping algorithm is to deform the initial surface based on the tissue classification and surface smoothness constraints. This is done in an iterative fashion. At each iteration, we compute a deformation vector for every surface point (mesh vertex). The deformation vector consists of two terms: one as

a result of the tissue types in its volumetric neighborhood (the *external* force), and the other as a result of the surface configuration in its surface neighborhood (the *internal* force).

The computation of the external and internal forces are similar to these presented in,[8] with the image intensity $I(\mathbf{x})$ replaced by the following function:

$$\mu(\mathbf{x}) = \mu_{GM}(\mathbf{x}) + \mu_{WM}(\mathbf{x}) - \mu_{CSF}(\mathbf{x}),$$

where $\mu_{GM}(\mathbf{x})$, $\mu_{WM}(\mathbf{x})$, and $\mu_{CSF}(\mathbf{x})$ are gray matter, white matter, and CSF membership functions. By modifying the image intensity based external force term into a tissue classification based one, we eliminate the dependency of surface deformation on a particular MR contrast. As we can see, in the above equation, the gray matter and white matter membership functions are combined. So the only assumption of our algorithm is that the MR protocol provides contrast between "solid" tissue and "fluid".

The internal force is derived from the triangulated mesh to enforce surface integrity and smoothness. As it is typical in parametric deformable surface models, this term has two parts: one in the tangent space of the surface, and one in the normal direction of the surface. The tangential component of the force moves a surface vertex towards the average location of the projections of its neighboring vertices in the tangent space; and therefore make the vertices evenly distributed on the surface. The normal component of the force moves a surface point towards the plane formed by its neighboring vertices to maintain the smoothness of the surface. As a consequence of the normal component, in locations where image evidence is weak in delineating the boundary between brain tissue and non-brain tissue, the boundary points estimated in its adjacent region can help predict the boundary point at the ambiguous locations.

The iterative process continues until either a maximal iteration number is reached or the average magnitude of the external force is small compared with that of the internal force.

3. RESULTS

We applied the skull stripping algorithm to all datasets from the OASIS database,[17] which includes 436 T1 weighted images and skull stripping results using Brain Extraction Tool (BET). Figure 3 shows an axial slice of a typical image from the database and its tissue segmentation, the union of GM (yellow), WM (red), and CSF (cyan) gives the brain mask, which we treat as ground truth in this paper.

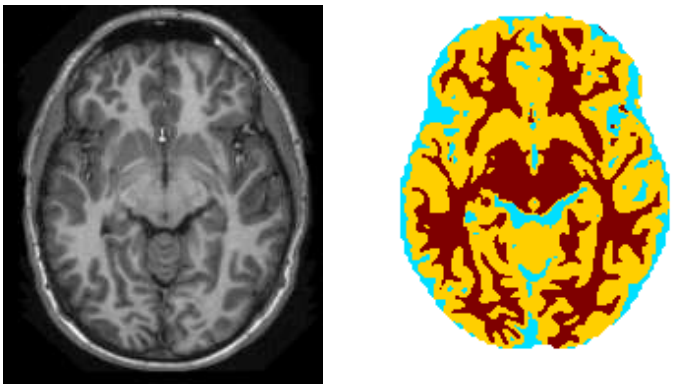

(a) (b)

Figure 3. (a) One axial slice of a typical OASIS dataset. (b) Tissue segmentation included in the OASIS database.

Figure 4 shows four typical skull stripping results overlaid on orthogonal views of T1 weighted image. The red curves are the intersection of the brain surface with the the orthogonal planes. Figure 5 shows a rendering of the brain surface. Figure 6 shows the deformable surface at different iteration numbers.

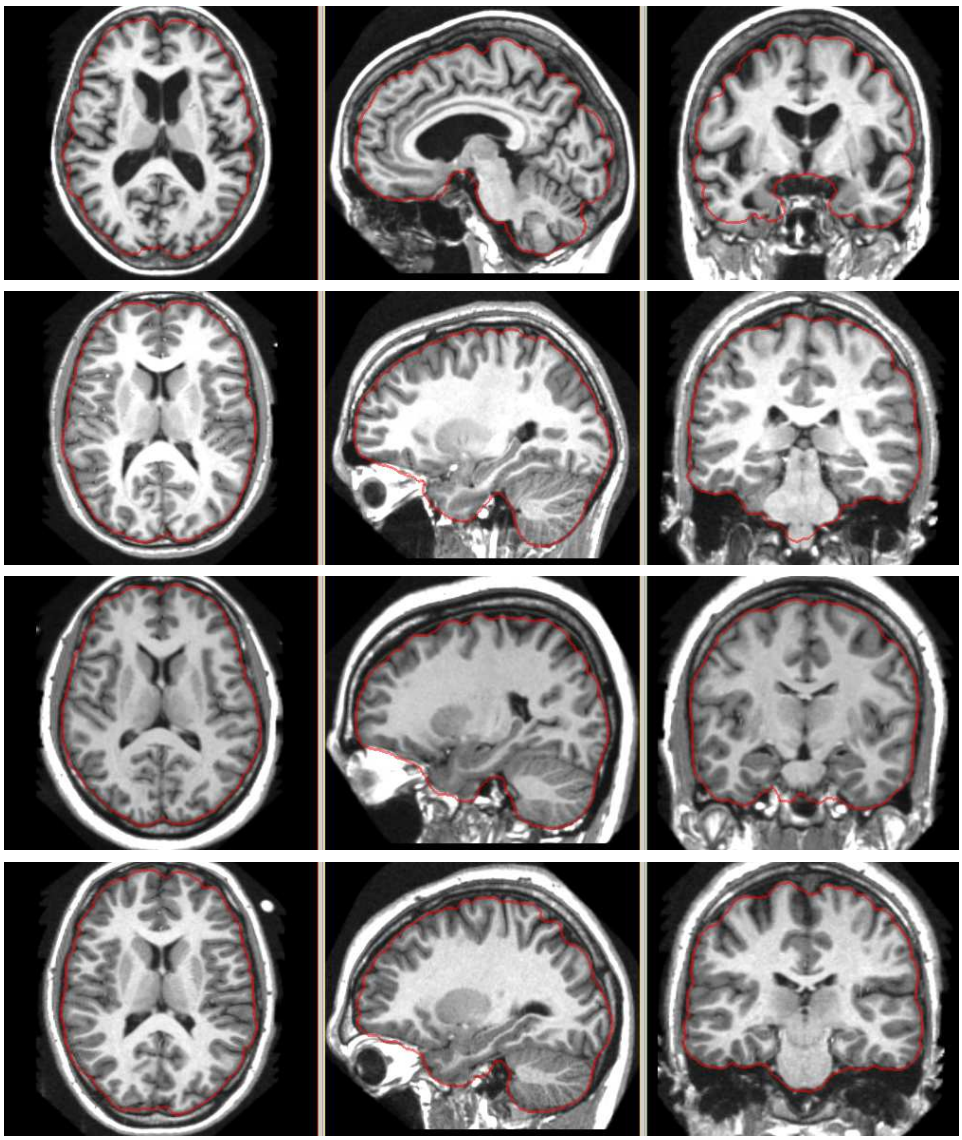

Figure 4. Four tyical skull stripping results shown as contours on orthogonal views of T1 weighted MR images.

We applied our algorithm to all datasets in the OASIS database and compared our skull stripping result with BET result by computing the *Dice similarity score*, which is defined as:

$$D = \frac{2 \times \#(M_{prop} \bigcap M_{BET})}{\#(M_{prop}) + \#(M_{BET})}$$

where M_{prop} is the brain mask obtained using the proposed algorithm, M_{BET} is the one in the OASIS database, and function $\#(\cdot)$ counts the number of voxels inside a mask. For all the datasets, the average Dice score is 0.948 with a standard deviation of 0.017.

In Figure 7, we compare our skull stripping result with the BET result on two slice views. We indicate the comparison in arrows where BET produced obvious errors, while the proposed algorithm gave more accurate results.

Figure 8 shows one skull stripping result on a T2 weighted image. This demonstrates the generality of the proposed algorithm in that it is capable to handle structural MR images with different contrasts.

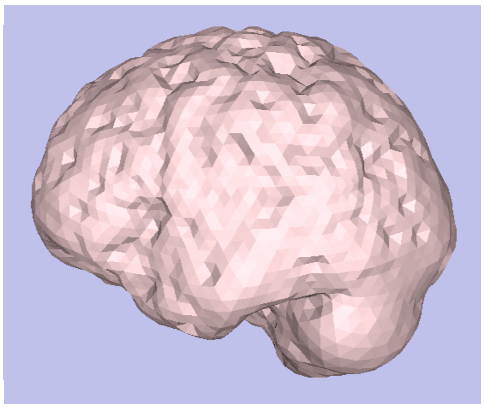

Figure 5. Surface rendering of the segmented brain.

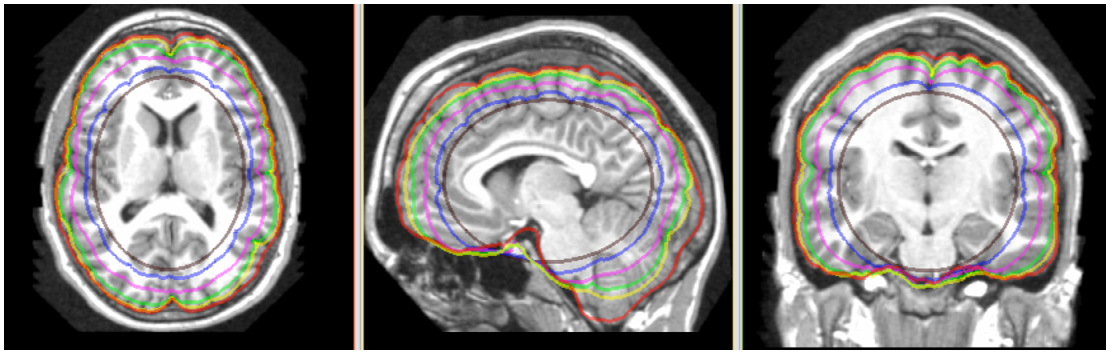

Figure 6. Surfaces at different deformation stages displayed on three orthogonal planes. From inside: initial surface, surfaces at 10th, 25th, 40th, 50th, and 800th iteration.

4. DISCUSSION AND CONCLUSION

We proposed an automated skull stripping algorithm using deformable surface models and fuzzy tissue classification. Because of the tissue classification, the algorithm can be applied to images with different tissue contrasts. The algorithm is robust to inhomogeneous gain field commonly observed in MR images due to the automatic gain field correction with a parametric bias field model in the tissue classification step. The algorithm is demonstrated on T1 weighted images and compared with BET skull stripping results with an average Dice score of 0.948. It is also successfully applied to a T2 weighted image.

In the future, we will improve the robustness of the algorithm to brains with degenerated conditions, for example, aged subject with wider sulcal space and abnormal contrasts. We would also like to conduct more thorough investigation of the performance of the algorithm on images from different data source.

ACKNOWLEDGMENTS

This work is part of the National Alliance for Medical Image Computing, funded by the National Institutes of Health through the NIH Roadmap for Medical Research, Grant U54 EB005149. Information on the National Centers for Biomedical Computing can be obtained from http://nihroadmap.nih.gov/bioinformatics. This work is also supported by Grant R01 EB006733 from the National Institute of Biomedical Imaging and Bioengineering , National Institutes of Health, through the University of North Carolina, Chapel Hill. All findings, opinions, and recommendations expressed in this paper are these of the authors and do not constitute these of the University of North Carolina, Chapel Hill or the National Institutes of Health.

REFERENCES

[1] Han, X., Pham, D., Tosun, D., Rettmann, M., Xu, C., and Prince, J., "CRUISE: Cortical Reconstruction Using Implicit Surface Evolution," *NeuroImage* **23**(3), 997–1012 (2004).

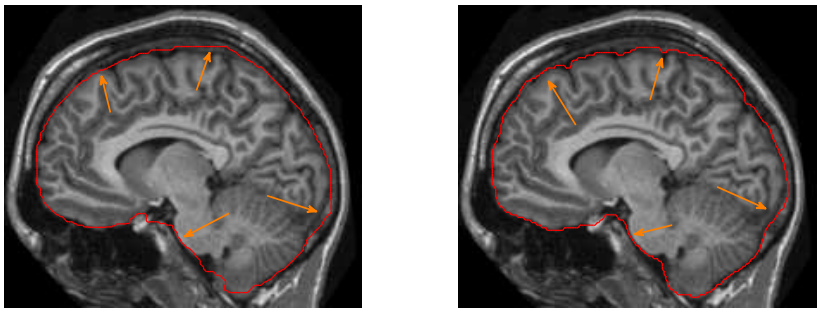

(a) (b)

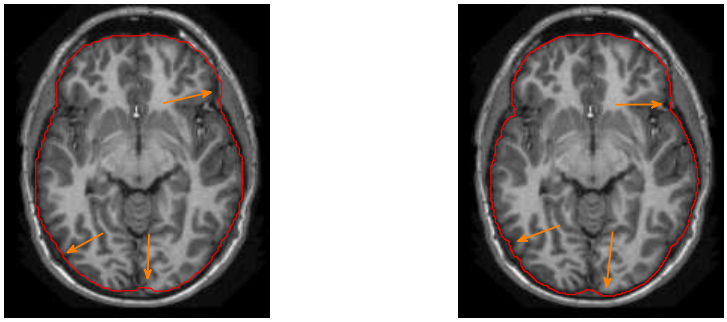

(c) (d)

Figure 7. One sagittal slice with BET skull stripping (a) and proposed skull stripping (b) results overlaid. One axial slice with BET skull stripping (c) and proposed skull stripping (d) results overlaid. Arrows point to the areas where BET either includes non-brain tissue, or cuts through cortical gray matters. These areas were correctly segmented using the proposed algorithm.

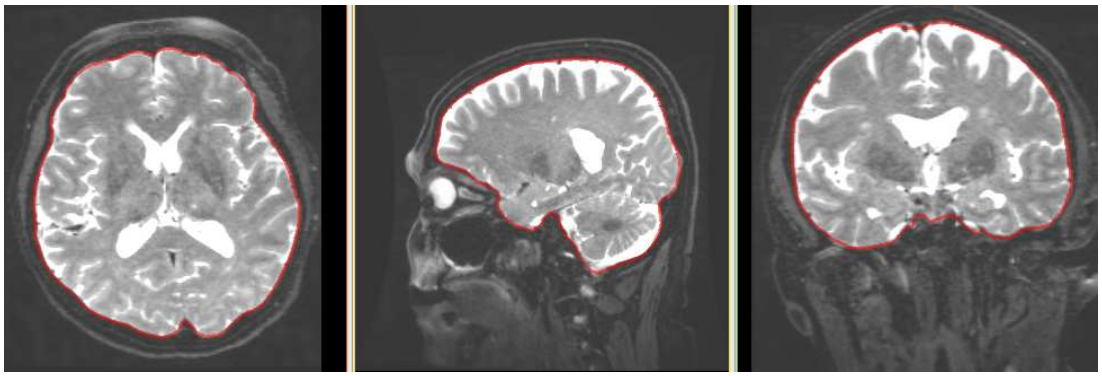

Figure 8. Skull stripping result on a T2 weighted image.

[2] Dickerson, B., Feczko, E., Augustinack, J., Pacheco, J., Morris, J., Fischl, B., and Buckner, R., "Differential effects of aging and Alzheimer's disease on medial temporal lobe cortical thickness and surface area," *Neurobiology of Aging* **30**(3), 432–440 (2009).

[3] Smith, S., De Stefano, N., Jenkinson, M., and Matthews, P., "Normalized accurate measurement of longitudinal brain change," *Journal of computer assisted tomography* **25**(3), 466 (2001).

[4] Kovalev, D., Spreer, J., Honegger, J., Zentner, J., Schulze-Bonhage, A., and Huppertz, H., "Rapid and fully automated visualization of subdural electrodes in the presurgical evaluation of epilepsy patients," *American Journal of Neuroradiology* **26**(5), 1078 (2005).

[5] Admiraal-Behloul, F., Van Den Heuvel, D., Olofsen, H., van Osch, M., van der Grond, J., Van Buchem, M., and Reiber, J., "Fully automatic segmentation of white matter hyperintensities in MR images of the elderly," *Neuroimage* **28**(3), 607–617 (2005).

[6] Lao, Z., Shen, D., Liu, D., Jawad, A., Melhem, E., Launer, L., Bryan, R., and Davatzikos, C., "Computer-Assisted Segmentation of White Matter Lesions in 3D MR images, Using Support Vector Machine," *Academic radiology* **15**(3), 300 (2008).

[7] Fennema-Notestine, C., Ozyurt, I., Clark, C., Morris, S., Bischoff-Grethe, A., Bondi, M., Jernigan, T., Fischl, B., Segonne, F., Shattuck, D., et al., "Quantitative Evaluation of Automated Skull-Stripping Methods Applied to Contemporary and Legacy Images: Effects of Diagnosis, Bias Correction, and Slice Location," *Human brain mapping* **27**(2), 99 (2006).

[8] Smith, S., "Fast Robust Automated Brain Extraction," *Human Brain Mapping* **17**(3) (2002).

[9] Goldszal, A., Davatzikos, C., Pham, D., Yan, M., Bryan, R., and Resnick, S., "An Image-Processing System for Qualitative and Quantitative Volumetric Analysis of Brain Images," *Journal of Computer Assisted Tomography* **22**(5), 827 (1998).

[10] Chiverton, J., Wells, K., Lewis, E., Chen, C., Podda, B., and Johnson, D., "Statistical Morphological Skull Stripping of Adult and Infant MRI Data," *Computers in Biology and Medicine* **37**(3), 342–357 (2007).

[11] Dale, A., Fischl, B., and Sereno, M., "Cortical Surface-Based Analysis: I. Segmentation and Surface Reconstruction," *Neuroimage* **9**(2), 179–194 (1999).

[12] Segonne, F., Dale, A., Busa, E., Glessner, M., Salat, D., Hahn, H., and Fischl, B., "A Hybrid Approach to the Skull Stripping Problem in MRI," *Neuroimage* **22**(3), 1060–1075 (2004).

[13] Carass, A., Wheeler, M., Cuzzocreo, J., Bazin, P., Bassett, S., and Prince, J., "A Joint Registration and Segmentation Approach to Skull Stripping," in [*4th IEEE International Symposium on Biomedical Imaging: From Nano to Macro (ISBI),*], 656–659 (2007).

[14] Chang, M.-C. and Tao, X., "Subvoxel Segmentation and Representation of Brain Cortex Using Fuzzy Clustering and Gradient Vector Diffusion," in [*SPIE Medical Imaging, Proceedings of SPIE Volume 7623*], (2010).

[15] Pham, D. L. and Prince, J. L., "Adaptive fuzzy segmentation of magnetic resonance images," *IEEE Trans. on Medical Imaging* **18**(9), 737–752 (1999).

[16] Bezdek, J., "A convergence theorem for the fuzzy ISODATA clustering algorithms," *IEEE Transactions on Pattern Analysis and Machine Intelligence* **2**(1), 1–8 (1980).

[17] Marcus, D., Wang, T., Parker, J., Csernansky, J., Morris, J., and Buckner, R., "Open Access Series of Imaging Studies (OASIS): Cross-Sectional MRI Data in Young, Middle Aged, Nondemented, and Demented Older Adults," *Journal of Cognitive Neuroscience* **19**(9), 1498–1507 (2007).